International Journal of Hydrogen Energy 81 (2024) 391–404

Contents lists available at ScienceDirect

International Journal of Hydrogen Energy

journal homepage: www.elsevier.com/locate/he

Ab initio study of the structural, mechanical, optoelectronic and thermo-physical properties of $XGaH_5$ (X=Ba, Ca, and Mg) compounds for hydrogen storage applications

Çağatay Yamçıçıer [a], Cihan Kürkçü [b,*]

[a] Department of Electricity and Energy, Osmaniye Korkut Ata University, Osmaniye, Turkey
[b] Department of Electronics and Automation, Kırşehir Ahi Evran University, Kırşehir, Turkey

ARTICLE INFO

Handling Editor: M Djukic

Keywords:
Hydrogen storage
Structural properties
Electronic properties
Elastic properties
Optical properties

ABSTRACT

The structural, mechanical, optical, thermo-physical, and electronic properties of the monoclinic $XGaH_5$ (X = Ba, Ca, and Mg) used as hydrogen storage material were investigated in detail using the ab initio technique. Gravimetric hydrogen densities (5.1 wt % for the $MgGaH_5$, 4.4 wt % for the $CaGaH_5$, and 2.38 wt % for the $BaGaH_5$), hydrogen desorption temperatures (29.05 K for the $MgGaH_5$, 175.56 K for the $CaGaH_5$, and 218.36 K for the $BaGaH_5$) and enthalpies of formation (−0.039 eV/atom for the $MgGaH_5$, -0.237 eV/atom for the $CaGaH_5$ and -0.296 eV/atom for the $BaGaH_5$) of these compounds were also calculated. As a result of electronic band structure calculations, band gap values for $BaGaH_5$, $CaGaH_5$, and $MgGaH_5$ were obtained as 3.08 eV, 4.05 eV, and 3.61 eV, respectively. It is clear from the high band gap values that all three materials have insulator character. The second-order independent elastic constant values, which provide information about the hardness and mechanical stability of the materials, were calculated. The elastic constant values showed that $XGaH_5$ is mechanically stable. Hardness parameters such as bulk modulus, shear modulus, B/G ratio (1.19 for the $MgGaH_5$, 1.11 for the $CaGaH_5$, and 1.68 for the $BaGaH_5$), Young's modulus, and Poisson's ratio were also calculated using elastic constant values. According to the B/G ratio, all three structures were found to be brittle materials. From Poisson's ratio (0.17 for the $MgGaH_5$, 0.15 for the $CaGaH_5$, and 0.25 for the $BaGaH_5$), the atoms in $XGaH_5$ compounds are connected by covalent bonds. Besides, the formation enthalpies of the materials were calculated, and it was concluded that all three compounds could be synthesized in the laboratory. In addition, some optical properties of $XGaH_5$ such as dielectric function, conductivity, reflectivity, and absorption were also calculated. Finally, thermo-physical properties were calculated for $XGaH_5$ compounds.

1. Introduction

The increasing population and energy need for daily requirements have caused concern among global policymakers, governments, and scientists. The exhaustion of oil reserves, fluctuating prices, and environmental damage resulting from production and consumption are major issues that require immediate focus and financial support. An urgent need exists to investigate energy sources that are plentiful, cost-effective, and environmentally sustainable [1–3]. Hydrogen energy is proposed and deemed crucial for tackling these concerns. Hydrogen can serve as an energy carrier in stationary power plants, fuel cells, and portable electronics [4].

One of the most important steps toward building the clean energy system of the future is finding materials that can store hydrogen [5–8]. Many people think that making more Pure Electric Vehicles (PEVs) and Hybrid Electric Vehicles (HEVs) is a good way to deal with these problems. Still, electric cars will only become popular if their battery systems work well and don't cost too much. The nickel-metal hydride (Ni/MH) secondary battery is a potential on-board battery system for long-term use. It has many benefits, such as the ability to handle overcharging and over-discharging, a high rate capacity, a high energy density, a long cycle life, and being environmentally friendly [9–12].

Different metals have been used to make materials better at absorbing and releasing hydrogen [13–17].

Various materials have been studied recently for their capacity to store hydrogen. Understanding the diverse attributes of hydrogen

* Corresponding author.
E-mail address: ckurkcu@ahievran.edu.tr (C. Kürkçü).

https://doi.org/10.1016/j.ijhydene.2024.07.276
Received 19 April 2024; Received in revised form 27 June 2024; Accepted 18 July 2024
Available online 24 July 2024
0360-3199/© 2024 Hydrogen Energy Publications LLC. Published by Elsevier Ltd. All rights are reserved, including those for text and data mining, AI training, and similar technologies.

storage materials is essential since each material displays unique hydrogenation/dehydrogenation processes. Thoroughly studying the physical properties of materials, such as crystal structures, hydrogenation capabilities, electronic characteristics, elastic properties, anisotropic properties, and thermodynamic properties, is essential to fully utilize the potential of hydrogen energy [18–20].

For example, we can get a sense of how the material would respond to hydrogen storage pressure by simulating how it acts under pressure. Using reversible hydrogen storage materials could make a big difference in how hydrogen is stored and how it is used in everyday life. It can also help lower the normal temperature around the world, which lessens the effects of global warming. Because of this, we still need to find new types of products.

According to the band gap values obtained as a result of electronic band structure calculations, $XGaH_5$ compounds have insulating properties. Insulating materials have some advantages when used in hydrogen storage. Compared to traditional methods, some insulators might boast higher energy density. This translates to storing more hydrogen in a smaller volume, making transportation and storage more efficient. Insulators generally weigh less than metals. This makes it much easier to transport and store hydrogen, especially crucial in weight-sensitive applications like aerospace. Certain insulators are relatively inexpensive, leading to a more budget-friendly storage option. Cost is a major factor, particularly for large-scale hydrogen storage systems. Insulators can potentially offer improved safety compared to traditional methods. Some insulators might not carry the risk of explosion or fire, leading to safer working environments. Insulators can be manufactured in various shapes and sizes. This flexibility allows them to be tailored to different hydrogen storage systems. Some insulators can be recycled and are environmentally friendly. This makes them an attractive option for sustainable hydrogen storage solutions. In essence, insulators offer a range of potential benefits for hydrogen storage, including higher energy density, lighter weight, lower costs, improved safety, design flexibility, and environmental friendliness. Research in this area is ongoing, and insulators could play a significant role in the future of hydrogen storage.

Moreover, dehydrogenation with $MgGaH_5$, $BaGaH_5$, and $CaGaH_5$ is also possible for portable applications. Dehydrogenation refers to the process of releasing hydrogen from a material. All three compounds mentioned ($MgGaH_5$, $BaGaH_5$, and $CaGaH_5$) have the potential to release hydrogen through dehydrogenation. This makes them candidates for hydrogen storage in portable applications.

There are studies on many different types of materials in this field [18,19,21]. In this study, density functional theory calculations have been used to look into the features of $XGaH_5$ compounds. This study aims to show that the use of insulation materials as hydrogen storage materials may be important. In addition, the comprehensive physical properties such as structural, elastic, electronic, dynamic, thermodynamic, and optic of the studied materials were calculated for the first time in this study. Besides, the calculated materials can also be used in portable applications. Moreover, it has also been calculated the enthalpies of formation, the temperatures at which hydrogen desorption, and the gravimetric hydrogen densities for the first time in this study.

Klaveness et al. [22] carried out a study titled "Coordination Preference of Ga in Hydrides" using the Vasp program. In their study, they mentioned some physical properties such as structural and electronic properties of $MGaH_5$ (M = Be, Mg, Ca, Sr, and Ba) compounds. There are no experimental and detailed theoretical studies on these compounds. For this reason, we carried out this study to learn the physical properties of $BaGaH_5$, $CaGaH_5$, and $MgGaH_5$ in detail and to pioneer future experimental studies. In light of this, this study will contribute greatly to the existing literature on solid-state hydrogen storage.

In Section 2, we talk about the ab initio method for computing. The structural properties of the $XGaH_5$, including its electronic band structure, density of states, mechanic properties, elastic anisotropy properties, thermo-physical properties, and optical properties, were determined and are shown in Sec.3. In Sec. 4, the conclusions are given.

2. Methods

The Siesta Package Program [23] was used to look at different physical properties of the $XGaH_5$ compounds, such as their structural, electronic properties, elastic, and optical properties. The Density Functional Theory was used to guide this research. The Perdew-Burke-Ernzerhof (PBE) function in the Generalized Gradient Approximation (GGA) [24] was used as exchange-correlation energy. Optimizations of the geometry were made before the calculations began. For the simulation study, the buildings that were the most stable and had the least amount of energy were chosen. All the calculations were done on these models as well. For the calculations, norm-conserving pseudopotentials of the Troullier Martins type were used for the Ba, Ca, Mg, Ga, and H atoms [25]. The valence electron configurations of the *Mg, Ca, Ba, Ga,* and *H* atoms in the mentioned systems are as follows: $3s^2, 4s^2, 6s^2, 4s^2 3d^{10} 4p^1, 1s^1$, respectively.

The calculations were also done using the double zeta polarized basis set. The mesh cut-off energy value was found to be 300 Raydberg after the optimization process. A k-point mesh and the Monkhorst-Pack method [26] were used to separate the Brillouin zones (BZ) for $XGaH_5$. For $BaGaH_5$, $CaGaH_5$, and $MgGaH_5$, the k-point meshes were used as 8x10x6, 6 × 8 × 6, and 10 × 8 × 6, respectively. It was used the conjugate-gradient (CG) method to improve the structure until the leftover force acting on all the atoms was less than 0.01 eV/Å^{-1}. The maximum atomic displacements and maximum force were set to 1.0 Å and 10–5 eV/atom, respectively. We used the Vesta program [27], which gives us a lot of information about the compounds we are studying, including their space group, lattice parameter values, and atomic positions. The volume conserving method and the Siesta program were used to find $XGaH_5$'s second-order independent elastic constant values [28].

3. Results and discussion

3.1. Structural properties

Fig. 1 shows the crystal structures of $MgGaH_5$, $CaGaH_5$, and $BaGaH_5$ compounds, respectively. $MgGaH_5$ crystallizes in a monoclinic structure with space group $P2_1/c$ (No. 14). The compounds $CaGaH_5$ and $BaGaH_5$ crystallize with space group $P2_1$ in the monoclinic structure (No. 4). $CaGaH_5$ and $BaGaH_5$ compounds have 14 atoms in the unit cell, while $MgGaH_5$ compound has 28 atoms in the unit cell. The fully relaxed structures for compound $XGaH_5$ (X = Mg, Ca, Ba) are achieved by optimizing the geometry, including lattice constants and atomic locations. Table 1 displays the lattice constants a, b, and c, angles α, β, and γ, equilibrium unit cell volume V, formation energy ΔH_f, and cohesive energy E_{coh} for $XGaH_5$ (X = Mg, Ca, Ba) under ambient pressure. In Tables 1 and it is seen that the results obtained are highly compatible with the previously theoretically performed studies in the literature [29,30]. Formation energy, which is an important parameter for hydrogen storage materials, is calculated from Equation (1) [4,31].

$$\Delta H_f = E_{tot}(XGaH_5) - E_{tot}(X) - E_{tot}(Ga) - \frac{5}{2}E_{tot}(H_2) \quad (1)$$

In equation (1), the total energy of the compounds $E_{tot}(XGaH_5)$, $E_{tot}(X)$, $E_{tot}(Ga)$ and $E_{tot}(H_2)$ represent the total energies of X (Mg, Ca, Ba), Ga, and H_2, respectively. The formation enthalpies for $MgGaH_5$, $CaGaH_5$, and $BaGaH_5$ were obtained to be −0.039, −0.237, and −0.296 eV/atom, respectively. The negative value of the enthalpy of formation is an indication that the calculated materials can be experimentally synthesized and are thermodynamically stable [32–35]. The fact that all calculated compounds have negative formation enthalpies indicates that these materials can be synthesized experimentally and are

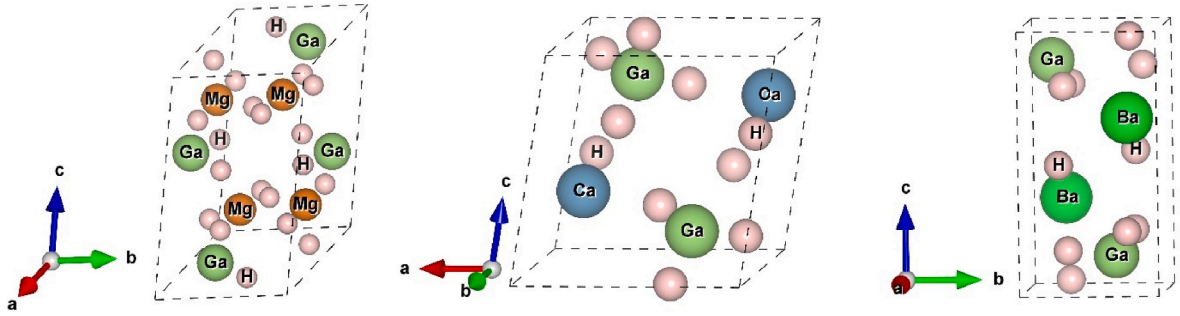

Fig. 1. Systematic crystal structures of $XGaH_5$ (X = Mg, Ca, Ba) hydrides with crystal axis directions.

Table 1
Lattice constants a, b, and c (Å), angles α, β, and γ, equilibrium unit cell volume V (Å^3), formation energy ΔH_f (eV/atom), and cohesive energy E_{coh}(eV/atom) for $XGaH_5$ (X = Mg, Ca, Ba).

Material	a	b	c	Angles	V	ΔH_f	E_{coh}	References
$MgGaH_5$	6.6190	6.9775	10.2796	α = 90.0000 β = 129.746 γ = 90.0000	365.04	−0.039	12.466	This study
	6.6140	6.9948	10.2739	α = 90.0000 β = 129.710 γ = 90.0000	365.64	–	–	[29]
$CaGaH_5$	6.6995	4.3709	6.7988	α = 90.0000 β = 102.805 γ = 90.0000	194.14	−0.237	6.697	This study
	6.5388	4.3136	6.6558	α = 90.0000 β = 102.973 γ = 90.0000	182.94	–	–	[29]
$BaGaH_5$	5.0135	4.6059	8.7177	α = 90.0000 β = 90.1383 γ = 90.0000	201.30	−0.296	6.807	This study
	5.0135	4.5869	8.6255	α = 90.0000 β = 90.1523 γ = 90.0000	198.35	–	–	[29]
	5.0230	4.6050	8.6447	α = 90.0000 β = 90.1310 γ = 90.0000	199.96	–	–	[30]

thermodynamically stable. $BaGaH_5$ was determined to be more stable because it had a greater negative formation enthalpy energy.

The cohesive energy (E_{coh}) is crucial for evaluating the stability of the system. This value indicates the strength of atomic bonds and represents the energy needed to separate a crystal into its components. The positive value of E_{coh} is an indication of the stability of the crystal. The cohesive energy formula for the $XGaH_5$ compound is shown in Equation (2) below.

$$E_{coh} = -\frac{1}{7}\left[E_{tot}(XGaH_5) - E_{tot}(X) - E_{tot}(Ga) - \frac{5}{2}E_{tot}(H_2)\right] \quad (2)$$

$E_{tot}(XGaH_5)$ represents the overall energy of $XGaH_5$, while $E_{tot}(X)$, $E_{tot}(Ga)$ and $E_{tot}(H_2)$ denote the energy of individual atoms within the unit cell. The results shown in Table 1 indicate that the heat release during the process is positive, suggesting a transition from individual atoms to compounds [36]. The results obtained show the thermodynamic stability of all materials tested. The bonded materials have higher cohesive energy, indicating that their thermodynamic stability is higher than that of the other materials.

3.2. Mechanical properties

Elastic constants are very important to describe the mechanical properties of materials. Understanding the elastic constants of crystalline solids is crucial for connecting the mechanical and dynamical aspects of crystals when subjected to various types of external stress. This knowledge is essential for determining the stability and stiffness of materials based on the forces at play in solids. There is a correlation between the elastic constants and the mechanical properties of a material, which include the material's stability, ductility, brittleness, stiffness, and elastic anisotropy. Engineers need to examine the mechanical characteristics of materials to obtain knowledge regarding the selection of materials. This information enables engineers to build structures and devices that can support particular loads and circumstances [37,38]. In the end, this knowledge allows for improvements in terms of safety, efficiency, and cost-effectiveness across a variety of applications. On the other hand, the elastic characteristics were determined by some distinct parameters, including crystal energy, equilibrium volume, and the strain-dependent matrix of second-order elastic constants (C_{ij}). All of the materials that are currently available have a monoclinic phase with a space group of $P2_1$ ve $P2_1/c$ and possess thirteen elastic stiffness tensors (C_{11}, C_{22}, C_{33}, C_{44}, C_{55}, C_{66}, C_{12}, C_{13}, C_{15}, C_{23}, C_{25}, C_{35}, and C_{46}). A monoclinic structure seriously adheres to the Born stability requirements and regards the materials as mechanically stable. Mechanical stability is expressed as [39–41]:

$$[C_{11} + C_{22} + C_{33} + 2(C_{12} + C_{13} + C_{23})] > 0,$$

$$C_{11} > 0, C_{22} > 0, C_{33} > 0, C_{44} > 0, C_{55} > 0, C_{66} > 0,$$

$$\left(C_{33}C_{55} - C_{35}^2\right) > 0, C_{44}C_{66} - C_{46}^2 > 0,$$

$$(C_{22} + C_{33} - 2C_{23}) > 0,$$

$$\left[C_{22}\left(C_{33}C_{55} - C_{35}^2\right) + 2\left(C_{23}C_{25}C_{35} - C_{23}^2C_{55} - C_{25}^2C_{33}\right)\right] > 0,$$

$$\{2[C_{15}C_{25}(C_{33}C_{12} - C_{13}C_{23}) + C_{15}C_{35}(C_{22}C_{13} - C_{12}C_{23}) + C_{25}C_{35}(C_{11}C_{23} - C_{12}C_{13})] - [C_{15}^2(C_{22}C_{33} - C_{23}^2) + C_{25}^2(C_{11}C_{33} - C_{13}^2) + C_{35}^2(C_{11}C_{22} - C_{12}^2)] + C_{55}(C_{11}C_{22}C_{33} - C_{11}C_{23}^2 - C_{22}C_{13}^2 - C_{33}C_{12}^2 + 2C_{12}C_{13}C_{23})\} > 0$$

Thus, the examined materials meet the Born stability criterion, as shown in Table 2. It was discovered that $XGaH_5$ (X = Mg, Ca, Ba) hydrides are mechanically stable.

Each elastic constant represents a distinct property; for instance, the ability to withstand linear compressions in the [100] and [001] orientations can be quantified by the elastic constants C_{11} and C_{33}, respectively. For the $MgCaH_5$ compound, C_{22} is larger than both C_{11} and C_{33}, indicating that the compressibility of the $MgCaH_5$ compound in terms of [010] is less. For $CaGaH_5$ and $BaGaH_5$ compounds, C_{11} is larger than C_{33} and C_{22}, indicating that these compounds are less compressible than other directions from [100]. Some elastic constants exhibit negative values in some non-diagonal elements due to the reduced symmetry present in the monoclinic phase [41,42]. The elastic constant C_{44} is used to indicate the resistance of the compound to shear deformation due to tangential stress applied in the [010] direction along the (001) plane. If it is found that C_{44} of the elastic constants fulfills the criterion of being smaller than (C_{11}, C_{22}, C_{33}), it can be concluded that sliding along any of the three crystallographic orientations can deform compounds more easily than unidirectional compression along the same directions. Looking at the values in Tables 2 and it can be said that $CaGaH_5$ and $BaGaH_5$ compounds are more susceptible to shear deformations because they satisfy this condition. However, the C_{44} value for the $MgGaH_5$ compound is larger than the C_{33} value, so it is not sensitive to shear deformation. The tetragonal shear modulus (C′) is a different measurement of the crystal's stiffness, and it is determined by the equation that is presented below:

$$C' = \frac{(C_{11} - C_{12})}{2} \tag{3}$$

This parameter defined in Equation (3) is a measure of the dynamic stability of materials. A value of the tetragonal shear modulus greater than zero indicates the dynamic stability of the materials, while a negative value is an indication of dynamic instability. As can be seen from Table 2, the tetragonal shear modulus was obtained as 22.50, 17.26, and 16.39 GPa for $MgGaH_5$, $CaGaH_5$, and $BaGaH_5$ compounds, respectively. The fact that the calculated materials have positive values shows that they are dynamically stable.

A dimensionless internal strain parameter also referred to as the Kleinman parameter (ζ), is a measurement that determines the stability of a compound with stretching and bending. To compute this parameter for $XGaH_5$ compounds, the equation that is presented below [43] has been utilized:

$$\zeta = \frac{C_{11} + 8C_{12}}{7C_{11} + 2C_{12}} \tag{4}$$

The value of the Kleinman parameter takes values between zero and one ($0 \leq \zeta \leq 1$). The higher limit of ζ represents the substantial contribution of bond bending to resist external stress, whereas the lower limit represents the significant contribution of bond stretching to resist external stress. The predicted ζ values for $MgGaH_5$, $CaGaH_5$, and $BaGaH_5$ are 0.26, 0.21, and 0.55 respectively. This suggests that the mechanical strength in $MgGaH_5$ and $CaGaH_5$ is mostly influenced by bond bending, while in $BaGaH_5$ it is influenced by bond stretching or shrinkage.

Cauchy pressure (C_P) is a significant mechanical characteristic of solids. The Cauchy pressure of a material is calculated as C_P=(C_{12} - C_{44}). Ductile materials are characterized by positive Cauchy pressure, while brittle materials are characterized by negative Cauchy pressure [44]. Cauchy pressure provides additional insight into the angular properties related to atomic bonding in a material [45]. Per Pettifor's rule [45], a material exhibiting a substantial positive Cauchy pressure and high ductility is characterized by a significant presence of metallic bonding. On the contrary, a substance exhibiting negative Cauchy pressure contains a higher proportion of angular bonds, resulting in increased brittleness and a significant presence of covalent bonding. Therefore, the negative Cauchy pressure values suggest that $MgCaH_5$, $CaGaH_5$, and $BaGaH_5$ exhibit brittleness and possess covalent bonding.

The bulk modulus (B) and shear modulus (G) of polycrystalline materials are determined using the Voigt-Reuss-Hill approximations [46–48]. The upper limits for the parameters expressed in terms of elastic coefficients (C_{ij}), which assume uniform stress in crystalline structures, are provided by the Voight approximation [47]. The Reuss [48] approximation assumes a uniform stress distribution, establishing the lower limit using the elastic compliance tensor S_{ij}. Reuss and Voigt's estimations of bulk and shear moduli closely approximate the lower and upper boundaries of real polycrystalline bulk and shear moduli. The Hill [46] approximation, which is the average of these two limits, offers a realistic description of polycrystalline bulk properties. The bulk modulus (B) and shear modulus (G) calculated using the Hill approach are defined from the following relationships [49].

$$B_H = \frac{B_V + B_R}{2} \tag{5}$$

$$G_H = \frac{G_V + G_R}{2} \tag{6}$$

Young's modulus (E) and poison ratio (ν), which can be calculated using the bulk modulus and shear modulus, are defined from the following equations.

$$E = \frac{9GB}{(3B + G)} \tag{7}$$

$$\nu = \frac{(3B - 2G)}{2(3B + G)} \tag{8}$$

Table 3 provides a summary of our mechanical property results. The mechanical properties of crystals can be assessed using the bulk and shear modulus. The bulk modulus B evaluates the crystals' resistance to volume deformation. The shear modulus G can forecast the resistance to plastic deformation. According to the low values of bulk and shear modulus in Table 3, $XGaH_5$ compounds ought to be soft, machinable materials. Therefore, the hardness values of these materials are expected to be low as well. Young's modulus quantifies the resistance of an elastic material to deformation in response to an applied force. As the Young's modulus of a material grows, its covalent nature also increases. $CaGaH_5$

Table 2
Computed elastic constants (C_{ij} in GPa), Cauchy pressure (C_p in GPa), tetragonal shear constant (C′ in GPa), and Kleinman parameter (ζ) of $XGaH_5$ (X = Mg, Ca, Ba).

Parameters	$MgGaH_5$	$CaGaH_5$	$BaGaH_5$
C_{11}	49.60	36.67	47.80
C_{22}	56.36	23.41	46.15
C_{33}	11.62	31.63	29.87
C_{44}	12.77	13.27	16.34
C_{55}	8.17	6.60	8.67
C_{66}	8.21	5.58	17.57
C_{12}	4.62	2.15	15.01
C_{13}	3.88	4.30	13.16
C_{15}	0.57	0.00	0.00
C_{23}	6.11	−1.12	13.94
C_{25}	0.35	0.00	0.00
C_{35}	0.12	0.00	0.00
C_{46}	−0.16	0.00	0.00
$C_P(C_{12}–C_{44})$	−8.20	−11.11	−1.33
C'	22.50	17.26	16.39
ζ	0.26	0.21	0.55

Table 3
Polycrystalline bulk moduli B_R, B_V, and B_H, shear moduli G_R, G_V, and G_H, Young's modulus E (all in GPa), Pugh's ratio B/G, Poisson's ratio υ and machinability index (μ^M) of $XGaH_5$ (X = Mg, Ca, Ba).

Compound	B_R	B_V	B_H	G_R	G_V	G_H	E	B/G	υ	μ^M
$MgGaH_5$	10.11	16.31	13.21	9.57	12.70	11.13	26.08	1.19	0.17	1.03
$CaGaH_5$	10.66	11.38	11.02	9.04	10.85	9.94	22.93	1.11	0.15	0.83
$BaGaH_5$	21.87	21.87	22.49	12.80	13.96	13.38	33.50	1.68	0.25	1.38

has a lower bulk modulus and Young's modulus compared to $MgGaH_5$ and $BaGaH_5$, respectively. $CaGaH_5$ has a lower Young's modulus value compared to $MgGaH_5$ and $BaGaH_5$, indicating that $CaGaH_5$ is less stiff than $MgGaH_5$ and $BaGaH_5$.

Pugh [50] introduced a well-known modulus ratio between bulk modulus, B, and shear modulus, G, referred to as Pugh's ratio, which distinguishes the failure mode (brittle and ductile) of materials. Pugh suggested a numerical method to differentiate between the brittleness and ductility of materials. The Pugh's ratio, B/G, indicates the ductility or brittleness of a material by comparing the bulk and shear moduli. A material exhibits ductile behavior when the Pugh's ratio value exceeds 1.75 and brittle behavior when the Pugh's ratio value is below 1.75. The (B/G) ratios for $MgGaH_5$, $CaGaH_5$, and $BaGaH_5$ are 1.19, 1.11, and 1.69, indicating that the compounds are probable to display brittle behavior. $BaGaH_5$ is anticipated to have a significantly higher level of brittleness.

Poisson's ratio (ν) is a parameter that quantifies the extent to which a material deforms (either expands or contracts) in response to the direction of loading. This metric is also used to measure the stability of solids against shear. The Poisson's ratio of a solid crystal has values between −1 and 0.5 ($-1.0 \leq \nu \leq 0.5$) [51]. When $\nu = 0.5$, elastic deformation does not impact volume [52]. This metric can predict if a material will exhibit brittleness or ductility based on a critical value of 0.26. If $\nu < 0.26$, the material is brittle; if $\nu > 0.26$, the material is ductile [53,54]. The Poisson's ratios for $MgGaH_5$ (0.17), $CaGaH_5$ (0.15), and $BaGaH_5$ (0.25) are all below 0.26, as shown in Table 3. We can therefore conclude that $MgGaH_5$, $CaGaH_5$, and $BaGaH_5$ possess brittleness. This corresponds to the result obtained from Pugh's ratio. Studying the value of ν allows for an analysis of the interatomic forces in solids [55,56]. If this ratio remains between 0.25 and 0.50, the central force interaction will be dominant. Otherwise, the non-central force will dominate. Therefore, we can say that for $MgGaH_5$ and $CaGaH_5$ compounds, non-central forces are dominant in the bonding of atoms.

One of the important parameters for engineering applications of solids is the machinability index (μ^M) [57]. Machinability refers to a solid's quality that influences the speed and ease with which it can be created using a cutting instrument. This trait is frequently utilized in engineering manufacturing and production. Work material, cutting tool, and cutting parameters each impact machinability differently [58]. The material's machinability determines the type of material, form, cutting force, feed rate, and depth of cut used in the cutting tool. Furthermore, it impacts the flexibility and dry lubricating properties of the solids [59,60]. The combination of high bonding strength and low shear resistance results in increased dry lubricity and good machinability. High plastic strain values, low feed forces, superior lubricating properties, and low friction are characteristics of materials with large values of μ^M. The following formula has been used to get the machinability index (μ^M):

$$\mu^M = \frac{B}{C_{44}} \tag{9}$$

$BaGaH_5$ has a higher μ^M compared to $MgGaH_5$ and $CaGaH_5$. The elastic moduli of $BaGaH_5$ are higher than those of $MgGaH_5$ and $CaGaH_5$, indicating that $BaGaH_5$ is more suited for tool applications than $MgGaH_5$ and $CaGaH_5$.Among the phases being studied, $BaGaH_5$ has the greatest μ^M value of 1.38, whereas $CaGaH_5$ has the lowest value.

3.3. Hardness

Hardness is a crucial characteristic of solids utilized in various technical applications. Hardness is a material's capacity to deform, exhibit plasticity, and demonstrate strength [61]. It is beneficial for comprehending the mechanical properties of solids. The hardness of a solid, which is connected to elastic moduli, can be determined using the following equations [57,62–65].

$$(H_V)_{miao} = \frac{(1-2\nu)\mathrm{E}}{6(1+\nu)} \tag{10}$$

$$(H_V)_{Chen} = 2\left[\left(\frac{G}{B}\right)^2 G\right]^{0.585} - 3 \tag{11}$$

$$(H_V)_{Tian} = 0.92\left(G/B\right)^{1.137} G^{0.708} \tag{12}$$

$$(H_V)_{Teter} = 0.151G \tag{13}$$

$$(H_V)_{Mazhnik} = \gamma_0 \chi(\sigma) E \tag{14}$$

$\chi(\sigma)$ Equation (14) is a function of the poison ratio and is calculated as follows:

$$\chi(\sigma) = \frac{1 - 8.5\sigma + 19.5\sigma^2}{1 - 7.5\sigma + 12.2\sigma^2 + 19.6\sigma^3}$$

Also γ_0 is a dimensionless constant with a value of 0.096.

The $(H_V)_{miao}$, $(H_V)_{Chen}$, $(H_V)_{Tian}$, $(H_V)_{Teter}$, and $(H_V)_{Mazhnik}$ values obtained for the $XGaH_5$ (X = Mg, Ca, Ba) compounds are presented in Table 4.

The hardness values obtained by various methods vary. The variations are anticipated due to the variable construction of the formulas, which are based on various elastic moduli (G, B, E) and Poisson's ratio. Mazhnik et al. [65] reported that hardness ratings might vary significantly depending on the calculation method using the elastic moduli of materials. We calculated the average hardness values of $XGaH_5$ (X = Mg, Ca, Ba) compounds to forecast their hardness. The average values for $XGaH_5$ (X = Mg, Ca, Ba) compounds are predicted to be 2.71 GPa, 2.67 GPa, and 2.14 GPa, respectively. The ranking of these compounds from lowest to highest in terms of their values is $BaGaH_5$ < $CaGaH_5$ < $MgGaH_5$. The calculated hardness values are in the range of 1.50–4.09 GPa, which suggests that all compounds under study are somewhat soft.

3.4. Elastic anisotropy

Material anisotropy refers to the direction-dependent qualities of a system when subjected to external stress, either elastic or mechanical, and is quantitatively measured. Most crystalline solid materials exhibit anisotropy. Various physical processes, such as plastic deformation growth in solids, crack propagation and development, internal friction, microscale cracking in ceramics, and phase transformations, are greatly influenced by the elastic anisotropy of crystalline materials [66,67]. Thus, from the perspective of practical applications, the study of the anisotropic behavior of solids is of great importance. Calculating the elastic anisotropy parameters for $XGaH_5$ (X = Mg, Ca, Ba) compounds is crucial to understanding their adaptability and potential applications

Table 4
Calculated hardness (GPa) based on elastic moduli and Poisson's ratio for $XGaH_5$ (X = Mg, Ca, Ba) hydrides.

Compound	$(H_V)_{Chen}$	$(H_V)_{Tian}$	$(H_V)_{Teter}$	$(H_V)_{Miao}$	$(H_V)_{Mazhnik}$	$(H_V)_{Avg}$
$MgGaH_5$	3.70	4.05	1.68	2.44	1.70	2.71
$CaGaH_5$	3.80	4.09	1.50	2.30	1.65	2.67
$BaGaH_5$	1.97	2.92	2.02	2.21	1.56	2.14

under various external stress conditions. All compounds being studied are elastically anisotropic since they show $C_{11} > C_{33}$. Monoclinic crystal systems are linked to three shear anisotropy factors, which can be determined using the following expressions [41]:

Shear anisotropy factor between ⟨011⟩ and ⟨010⟩ directions for shear plane {100},

$$A_1 = \frac{(C_{11} + C_{12} + 2C_{33} - 4C_{13})}{6C_{44}} \tag{13}$$

Shear anisotropy factor between ⟨101⟩ and ⟨001⟩ directions for shear plane {010},

$$A_2 = \frac{2C_{44}}{C_{11} - C_{12}} \tag{14}$$

Shear anisotropy factor between ⟨110⟩ and ⟨010⟩ directions for shear plane {001},

$$A_3 = \frac{(C_{11} + C_{12} + 2C_{33} - 4C_{13})}{3(C_{11} - C_{12})} \tag{15}$$

The factors $A_{1,2,3}$ must be equal to one for isotropic crystals. $A_{1,2,3}$'s deviation from the non-unity value indicates the level of elastic anisotropy in shear. The $A_{1,2,3}$ values have been displayed in Table 5 for the structures under study, all of which exhibit strong anisotropy.

The formulae provided are used to calculate the universal anisotropy index (A^U and d_E), Zener anisotropy measure (A^{eq}), shear anisotropy (A_G), and anisotropy in compressibility of materials with any crystal symmetry (A_B) [66,68–70].

$$A^U = \frac{B_V}{B_R} + 5\frac{G_V}{G_R} - 6 \geq 0 \tag{16}$$

$$d_E = \sqrt{A^U + 6} \tag{17}$$

$$A^{eq} = \left(1 + \frac{5}{12}A^U\right) + \sqrt{\left(1 + \frac{5}{12}A^U\right)^2 - 1} \tag{18}$$

$$A_B = \frac{B_V - B_R}{B_V + B_R} \tag{19}$$

$$A_G = \frac{G_V - G_R}{G_V + G_R} \tag{20a}$$

The Universal Anisotropy Index (A^U) is a commonly used metric for measuring anisotropy in elastic characteristics. It is a unique measure of anisotropy that is independent of crystal symmetry. A^U is the initial anisotropy parameter that accounts for both shear and bulk contributions, distinguishing it from all other current anisotropy parameters. An isotropic material has an A^U value of zero, while a value different from zero indicates different levels of anisotropy. The computed A^U values for $MgGaH_5$, $CaGaH_5$, and $BaGaH_5$ are 2.247, 1.070, and 0.511 respectively, indicating anisotropic characteristics.

The value of A^{eq} is equal to 1.0 for isotropic crystals. Values of A^{eq} other than one indicate the extent of anisotropy. The values of A^{eq} for the compounds in the study were obtained as 3.594, 2.490, and 1.900 for $MgGaH_5$, $CaGaH_5$, and $BaGaH_5$ respectively, and are presented in Table 5.

A_B and A_G values have values between 0 and 1. Values of shear anisotropy and compressibility anisotropy equal to 0 provide the perfect elastic isotropy ($A_B = A_G = 0$), while values of these values equal to 1 provide the maximum elastic anisotropy ($A_B = A_G = 1$). For the $MgGaH_5$ compound, the larger value of A_B compared to A_G indicates that the anisotropy in compressibility is larger than the anisotropy in shear. However, for $CaGaH_5$ and $BaGaH_5$, the A_G value is larger than the A_B value, indicating that the shear anisotropy is larger than the compressibility anisotropy in these compounds.

The log-Euclidean formula is used to determine the universal log-Euclidean index [71]:

$$A^L = \sqrt{\left[\ln\left(\frac{B_V}{B_R}\right)\right]^2 + 5\left[\ln\left(\frac{C_{44}^V}{C_{44}^R}\right)\right]^2} \tag{20b}$$

The constants $C_{44}^R = \frac{5}{3}\frac{C_{44}(C_{11}-C_{12})}{3(C_{11}-C_{12})+4C_{44}}$ and $C_{44}^V = \frac{3}{5}\frac{(C_{11}-C_{12}-2C_{44})}{3(C_{11}-C_{12})+4C_{44}}$ are the Reuss and Voigt approximations for the elastic constant C_{44}, respectively. Kube and Jong [66,72] reported that the A^L value ranges from 0 to 10.26 for inorganic crystals and about ninety percent of the compounds have A^L values less than one. Additionally, the majority (78%) of these inorganic crystalline compounds with high A^L values exhibit layered or lamellar structures [73]. Large values of A^L indicate a strong layered structure, while low values of A^L indicate a non-layered structure. The low A^L value indicates that $XGaH_5$ lacks distinct layered characteristics. When perfect isotropy is present, the value of A^L is equal to zero. Among the $MgGaH_5$, $CaGaH_5$, and $BaGaH_5$ compounds, the estimated values of A^L are 0.674, 0.127, and 0.055, respectively. These values are all less than 1, which indicates that the anisotropy is moderate.

To determine linear compressibility along the a and c axes, the following equation is utilized for the computation [74]:

$$\frac{k_c}{k_a} = f = \frac{C_{11} + C_{12} - 2C_{13}}{C_{33} - C_{13}} \tag{21}$$

The f value is a critical characteristic that dictates whether a material is isotropic or anisotropic. If the f value equals 1, the material is considered isotropic. If the f value is not equal to 1, it suggests that the material is anisotropic. The results in Table 5 show that the $XGaH_5$ (X = Mg, Ca, Ba) compounds display anisotropic behavior. The data in Table 5 is distinctive and lacks any preexisting estimates for comparison.

The equations defining the bulk modulus along the a, b, and c axes and their anisotropies are as follows [71].

Table 5
Shear anisotropic factors (A_1, A_2, and A_3), anisotropy in compressibility A_B, anisotropy in shear A_G, the universal anisotropy index A^U and d_E, equivalent Zener anisotropy measure A^{eq}, universal log-Euclidean index A_L and linear compressibility (K_c/K_a) for $XGaH_5$ (X = Mg, Ca, Ba) hydrides.

Parameters	$MgGaH_5$	$CaGaH_5$	$BaGaH_5$
A_1	0.808	1.066	0.713
A_2	0.568	0.769	0.997
A_3	0.459	0.820	0.711
A_B	0.235	0.032	0.028
A_G	0.140	0.091	0.043
A^U	2.247	1.070	0.511
d_E	2.872	2.659	2.552
A^{eq}	3.594	2.490	1.900
A^L	0.674	0.127	0.055
K_c/K_a	6.002	1.105	2.185

$$B_a = a\frac{dP}{da} = \frac{\mathrm{D}}{1+\alpha+\beta}, B_b = b\frac{dP}{db} = \frac{B_a}{\alpha}, B_c = c\frac{dP}{dc} = \frac{B_a}{\beta} \quad (22)$$

Where $\mathrm{D} = C_{11} + 2C_{12}\alpha + C_{22}\alpha^2 + 2C_{13}\beta + C_{33}\beta^2 + 2C_{23}\alpha\beta$ and

$$\alpha = \frac{\{(C_{11}-C_{12})(C_{33}-C_{13})\} - \{(C_{23}-C_{13})(C_{11}-C_{13})}{\{(C_{33}-C_{13})(C_{22}-C_{12})\} - \{(C_{13}-C_{23})(C_{12}-C_{23})\}}$$

$$\beta = \frac{\{(C_{22}-C_{12})(C_{11}-C_{13})\} - \{(C_{11}-C_{12})(C_{23}-C_{12})\}}{\{(C_{22}-C_{12})(C_{33}-C_{13})\} - \{(C_{12}-C_{23})(C_{13}-C_{23})\}}$$

The B_b value for the $MgGaH_5$ compound is considerably higher than the B_a and B_c values. This means that the compressibility of the $MgGaH_5$ compound in the b direction is more difficult than in the a and c directions. For the $CaGaH_5$ compound, the B_a value is considerably higher than the B_b and B_c values. This means that the compressibility of the $CaGaH_5$ compound in a direction is more difficult than in the b and c directions. For the $BaGaH_5$ compound, the values of B_a and B_b are almost equal and larger than the value of B_c. This means that the compressibility of the $BaGaH_5$ compound in the a and b directions is more difficult than in the c direction. The data in Table 6 are novel and lack any existing comparative data in the literature.

$$A_{B_a} = \frac{B_a}{B_b}, A_{B_c} = \frac{B_c}{B_b} \quad (23)$$

For $MgGaH_5$ and $CaGaH_5$ compounds, the values of A_{B_a} and A_{B_c} are different from 1, indicating the presence of anisotropy in the axial bulk modulus. Table 6 data shows that the value of A_{B_a} is 1 for $BaGaH_5$ compounds, suggesting isotropy in the axial bulk modulus. However, A_{B_c} has a value different from 1, which indicates anisotropy in the axial bulk modulus.

We used the VELAS [75] code to estimate the direction-dependent variation of Young's modulus, shear modulus, bulk modulus, and Poisson's ratio to depict elastic anisotropy in more detail. Fig. 2 displays a 3D plot showing Young's modulus, bulk modulus, shear modulus, and Poisson's ratio. 3D contour plots should exhibit spherical symmetry for isotropic crystals; otherwise, they indicate the presence of anisotropy. Fig. 2 displays deviations from a spherical shape in the 3D representations of Young's modulus, bulk modulus, shear modulus, and Poisson's ratio indicating anisotropy. Table 7 displays the maximum and minimum values of Young's modulus, bulk modulus, and shear modulus along with their corresponding ratios. These ratios are valuable indicators of elastic anisotropy.

3.5. Optical properties

One of the most crucial aspects of solid crystals is their optical properties, which show how a material responds to incident electromagnetic radiation. The ability to respond to visible light is critical in optoelectronic applications. For example, materials with high transparency and low absorption in the visible spectrum are ideal for applications such as photovoltaics, displays, and sensors. Additionally, the ability of a material to efficiently convert light into electrical signals is essential for devices like photodetectors and solar cells. Therefore, understanding and optimizing the optical properties of materials is essential for the development of advanced optoelectronic technologies. The optical properties of a material, such as the dielectric function, optical conductivity, absorption coefficient, and reflectivity, which are dependent on energy and frequency, can fully characterize how the material reacts to incoming light. These properties are essential in understanding how materials interact with electromagnetic radiation across different wavelengths. By analyzing the dielectric function, for example, researchers can gain insight into the material's ability to respond to an applied electric field. The optical conductivity helps to determine how well a material can conduct electricity when exposed to light. Additionally, the absorption coefficient and reflectivity provide information on how much light is absorbed or reflected by the material, which is crucial for applications in various fields such as solar energy harvesting and photovoltaics. We have investigated the optical properties of $XGaH_5$ compounds in various energy ranges along [100] the polarization direction of the electric field as shown in Fig. 3(a–d).

Table 6
Bulk modulus (in GPa) B_a, B_b, and B_c along crystallographic axes a, b, and c, respectively. The anisotropy of linear bulk moduli (A_{B_a} and A_{B_c}) along a and c axes for $XGaH_5$ (X = Mg, Ca, Ba) hydrides.

Compound	B_a	B_b	B_c	α	β	A_{B_a}	A_{B_c}
$MgGaH_5$	74.08	119.48	12.99	0.62	5.70	0.62	0.11
$CaGaH_5$	48.54	24.45	31.25	1.99	1.55	1.99	1.28
$BaGaH_5$	88.38	88.46	43.73	1.00	2.02	1.00	0.49

The relationship between the electronic band structure and the imaginary component [$\varepsilon_2(\omega)$] of the dielectric function is direct. This component can be predicted using a permitted transition from one electronic state to another in the Brillouin zone and the momentum matrix element. Kramers-Kronig relations provide the real part [$\varepsilon_2(\omega)$] of the dielectric function based on the imaginary part. The real and imaginary part of the dielectric function is obtained from the following equations [76–80].

$$\varepsilon_1(\omega) = 1 + \frac{2}{\pi}\int_0^{\infty}\frac{\varepsilon_2(\omega')\omega' d\omega'}{\omega'^2-\omega^2} \quad (24)$$

$$\varepsilon_2(\omega) = \frac{2e^2\pi}{\Omega\varepsilon_0}\sum_{k,v,c}\left|\psi_k^c\middle|\mathbf{u}\bullet\mathbf{r}\middle|\psi_k^v\right|^2\delta\left(E_K^C - E_K^V - E\right) \quad (25)$$

$$n(\omega) = \frac{1}{\sqrt{2}}\left[\left\{\varepsilon_1(\omega)^2 + \varepsilon_2(\omega)^2\right\}^{1/2} + \varepsilon_1(\omega)\right]^{1/2} \quad (26)$$

$$k(\omega) = \frac{1}{\sqrt{2}}\left[\left\{\varepsilon_1(\omega)^2 + \varepsilon_2(\omega)^2\right\}^{1/2} - \varepsilon_1(\omega)\right]^{1/2} \quad (27)$$

$$R(\omega) = \left|\frac{\tilde{n}-1}{\tilde{n}+1}\right| = \frac{(n-1)^2+k^2}{(n+1)^2+k^2} \quad (28)$$

$$a(\omega) = \frac{4\pi k(\omega)}{\lambda} \quad (29)$$

$$\sigma(\omega) = \frac{2W_{cv}\hbar\omega}{\vec{E}_0^{\,2}} \quad (30)$$

Fig. 3 (a) displays the real (Re) and imaginary (im) components of the dielectric function for XGaH5 (X = Mg, Ca, Ba). The static dielectric functions of $MgGaH_5$, $CaGaH_5$, and $BaGaH_5$ are 3.42, 3.40, and 3.98, respectively, as shown in Fig. 3(a). The $BaGaH_5$ compound has the highest static dielectric constant, suggesting it exhibits the most polarization when compared to $MgGaH_5$ and $CaGaH_5$. The dielectric function (real) of $XGaH_5$ (X = Mg, Ca, Ba) hydrides increases gradually as the incident photon energy value increases. The real part of the dielectric functions of $MgGaH_5$, $CaGaH_5$, and $BaGaH_5$ hydrides reaches maximum peak values of 4.83 eV at 6.11, 4.86 eV at 6.50 and 3.87 eV at 6.51, respectively. $MgGaH_5$, $CaGaH_5$, and $BaGaH_5$ hydrides reached their minimum values at −0.68 at 8.61 eV, −0.55 at 10.54 eV, and −1.52 at 31.68 eV, respectively. The negative values of $XGaH_5$ (X = Mg, Ca, Ba) hydrides confirm the plasma response [81]. The fact that the imaginary part of the dielectric function of $XGaH_5$ (X = Mg, Ca, Ba) hydrides does not start at 0 eV indicates that these hydrides have a band gap. The imaginary component of the dielectric function for $MgGaH_5$, $CaGaH_5$, and $BaGaH_5$ peaks at 6.01, 5.89, and 5.30 eV, respectively. Overall, the examination of the dielectric function shows that all materials respond to low photon energy levels.

The optical conductivity, represented by σ(ω), refers to how an

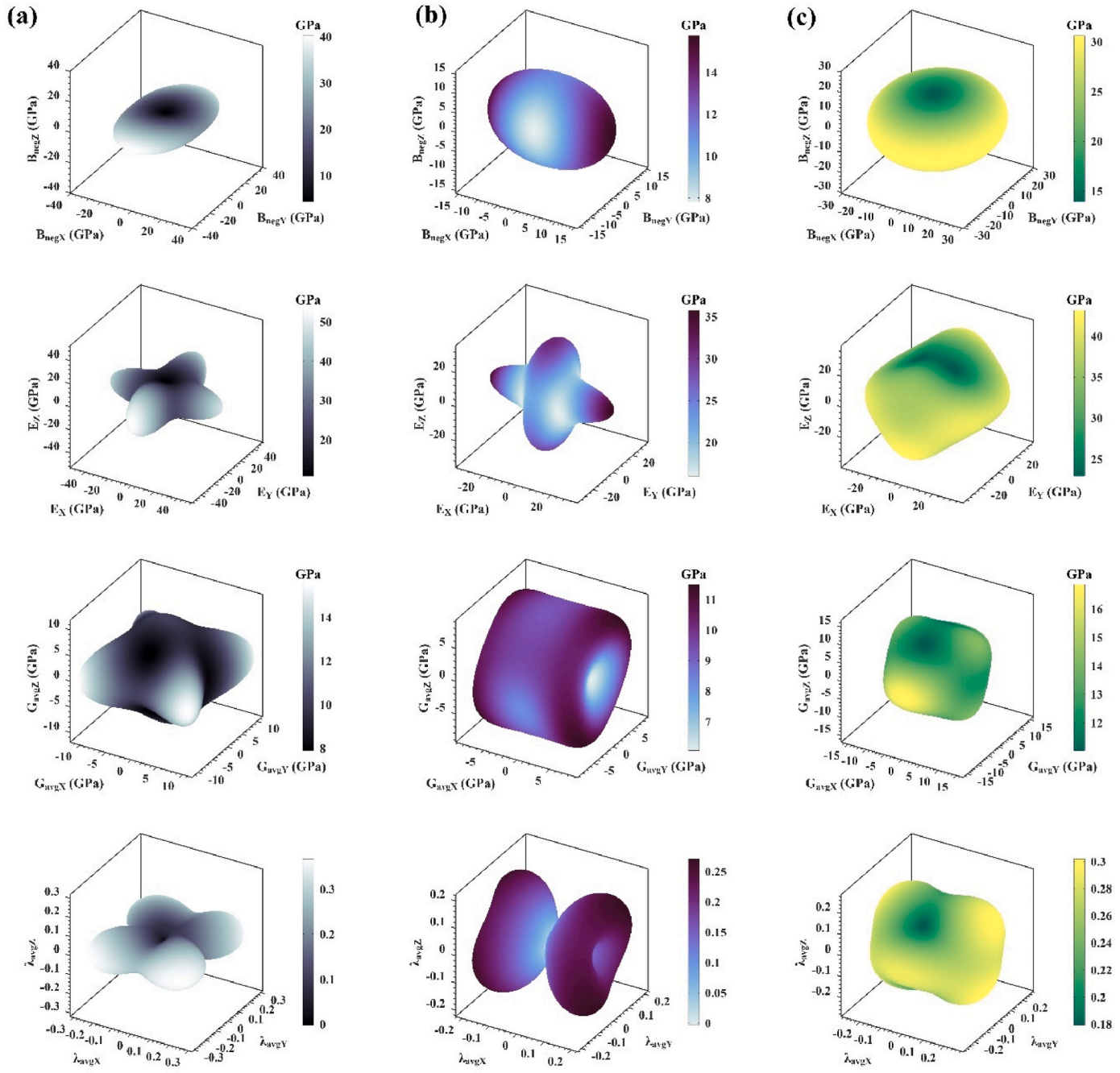

Fig. 2. 3D directional dependences of Bulk modulus, Shear modulus, Young modulus, and Poisson's ratio for (a) $MgGaH_5$, (b) $CaGaH_5$, (c) $BaGaH_5$.

Table 7
Maximum, minimum, and anisotropy values of Young's modulus, linear compressibility, and shear modulus values for $XGaH_5$ (X = Mg, Ca, Ga) compounds.

Compound	E_{min}	E_{max}	A_E	β_{min}	β_{max}	A_β	G_{min}	G_{max}	A_G
$MgGaH_5$	10.73	53.00	0.46	8.29	77.28	0.53	6.70	24.02	0.24
$CaGaH_5$	15.99	35.78	0.20	7.82	15.75	0.15	5.38	14.81	0.21
$BaGaH_5$	22.92	43.16	0.21	13.93	30.63	0.28	8.67	17.57	0.17

electromagnetic field stimulates electron conduction. Fig. 3 (b) shows the σ(ω) value derived using the dielectric function. As can be seen from Fig. 3(b), $XGaH_5$ (X = Mg, Ca, Ba) hydrides do not start at 0 eV; This shows that it is in agreement with the electronic band structure and density state calculations. Although the maximum values of the optical conductivity are observed in the vacuum ultraviolet region at 6.22 and 6.9 eV for $MgGaH_5$ and $CaGaH_5$, respectively, the maximum value for $BaGaH_5$ is observed in the extreme ultraviolet region at 30.80 eV.

Reflectance is the quantity of light that an object or material reflects when exposed to light. The value goes from 0 to 1, where 0 indicates complete absorption of light and 1 indicates complete reflection of light. Fig. 4 (a) displays the reflectance of $XGaH_5$ (X = Mg, Ca, Ba) hydrides within the photon energy range of 0–45 eV. The zero-frequency reflectivity R (0) of $MgGaH_5$, $CaGaH_5$, and $BaGAH_5$ is 0.31, 0.27 and 0.91

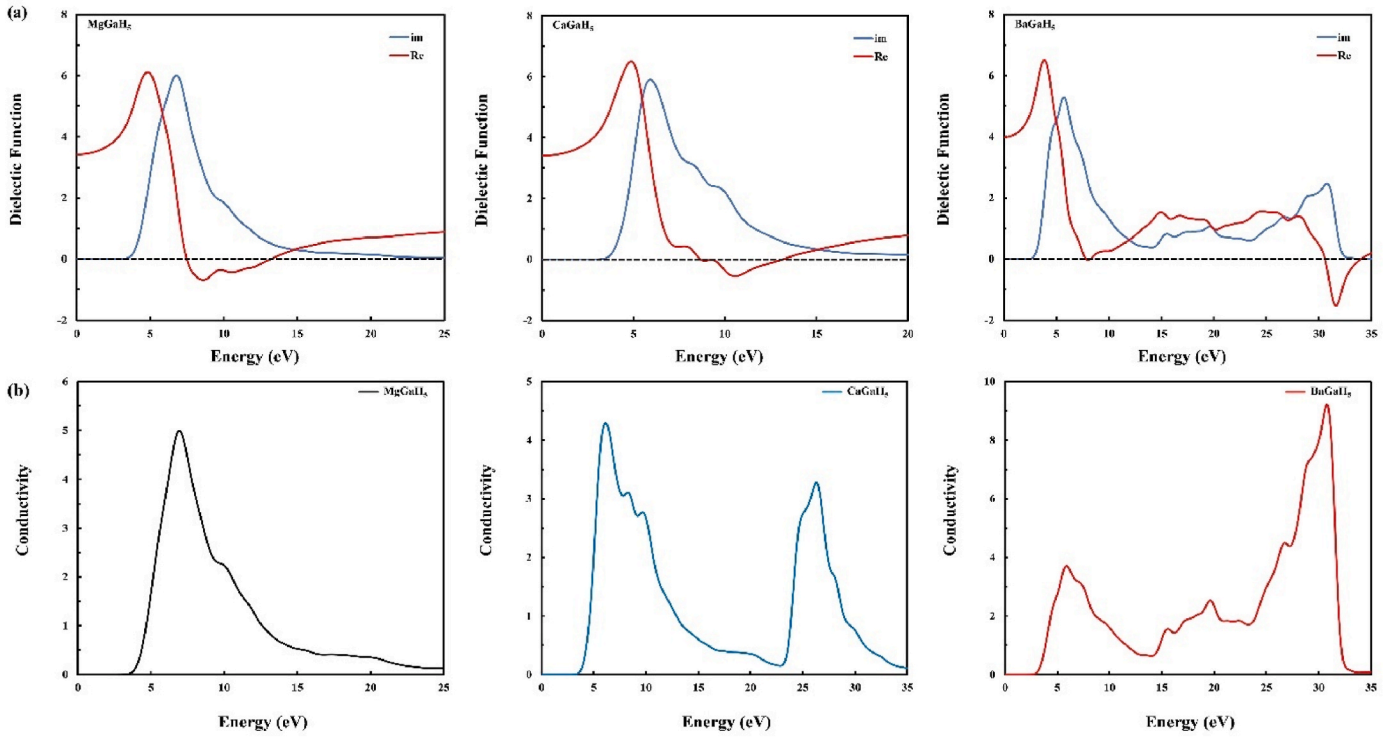

Fig. 3. (a) Real and imaginary part of the dielectric function and (b) conductivity for $XGaH_5$ (X = Mg, Ca, Ba) hydrides.

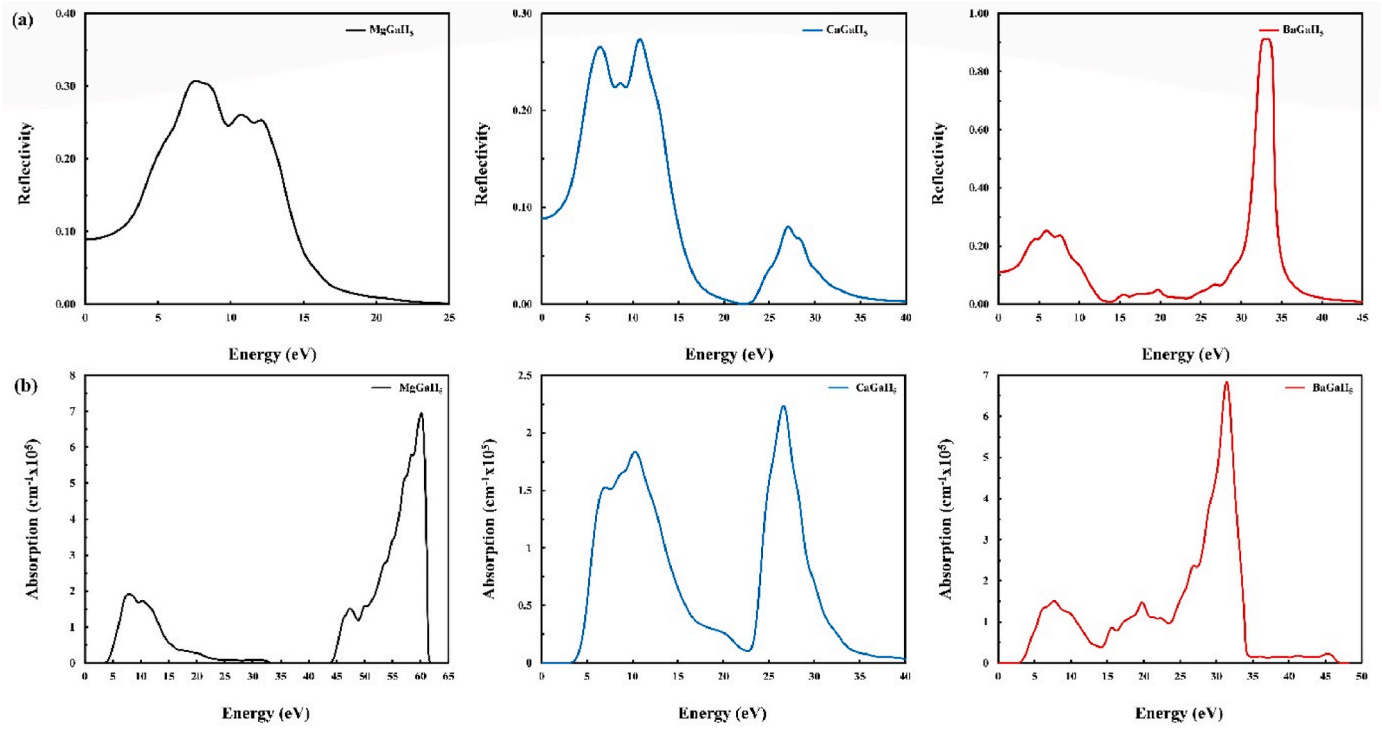

Fig. 4. (a) Reflectivity and (b) absorption coefficient for $XGaH_5$ (X = Mg, Ca, Ba) hydrides.

respectively. The maximum reflectivity of $MgGaH_5$, $CaGaH_5$, and $BaGaH_5$ is 31% at 7.58 eV, 27% at 10.77 eV, and 91% at 32.87 eV, respectively. Electromagnetic radiation in the visible area with a polarization of [100] has a reflectance of under 40%. $XGaH_5$ can be used as an anti-reflection material for this polarization.

Optical absorption qualities are crucial to the performance of optoelectronic and photovoltaic materials because they facilitate the creation and transmission of charge carriers via light absorption. Fig. 4 (b) shows the $XGaH_5$ hydrides absorption coefficient. $XGaH_5$ hydrides have peaks in the vacuum ultraviolet and extreme ultraviolet region. The maximum absorption coefficient for $MgGaH_5$, $CaGaH_5$, and $BaGaH_5$ hydrides is 1.91×10^5 cm^{-1} at 7.8 eV, 1.84×10^5 cm^{-1} at 10.30 eV and

1.51 × 10^5 cm^{-1} at 7.73 eV in the vacuum ultraviolet region, respectively. The maximum peaks in the extreme ultraviolet region of the absorption coefficient were obtained as 6.95 × 10^5 cm^{-1} at 60.17 eV, 2.24 × 10^5 cm^{-1} at 26.6 eV, and 6.84 × 10^5 cm^{-1} at 31.42 eV for $MgGaH_5$, $CaGaH_5$ and $BaGaH_5$ hydrides, respectively. These findings suggest that XGaH5 exhibits high absorption of vacuum far ultraviolet radiation, making it a promising optoelectronic material.

3.6. Thermo-physical properties

Debye temperature (θ_D) is a thermo-physical parameter influencing physical properties like thermal conductivity, lattice vibration, and interatomic bonding. Compounds with stronger bonds, lower mass, higher melting point, and higher mechanical wave velocity have higher Debye temperature. The Debye temperature can be calculated using the subsequent equation from the average speed of sound [82].

$$\theta_D = \frac{h}{k_B}\left[\left(\frac{3N}{4\pi}\right)\frac{N_A\rho}{M}\right]^{\frac{1}{3}} v_m \tag{26}$$

The variables in this equation are Planck's constant (h), Boltzmann constant (k_B), Avogadro's number (N_A), density (ρ), molecular weight (M), number of atoms (N), and mean sound velocity (v_m). The equation shows that θ_D is proportional to the mean sound velocity, which is determined by a crystal's elastic properties. The average speed of sound, v_m, in the crystal is determined using the following formula [83]:

$$v_m = \left[\frac{1}{3}\left(\frac{2}{v_t^3}+\frac{1}{v_l^3}\right)\right]^{-\frac{1}{3}}, v_t = \sqrt{\frac{G}{\rho}}, v_l = \sqrt{\frac{3B+4G}{3\rho}} \tag{27}$$

Here v_t and v_l are the longitudinal and transverse modes of the sound velocities which can be calculated from the bulk modulus and shear modulus. The calculations for ρ, θ_D, v_m, v_l and v_t for $XGaH_5$ hydrides are presented in Table 8. Increased Debye temperature values indicate stronger chemical bonding and greater phonon thermal conductivity. The Debye temperatures for $MgGaH_5$, $CaGaH_5$, and $BaGaH_5$ are 345.96 K, 306.24 K, and 265.83 K, respectively, as shown in Table 8. $MgGaH_5$ has a higher Debye temperature compared to $CaGaH_5$ and $BaGaH_5$, indicating stronger chemical bonding and greater phonon thermal conductivity.

The melting temperature, T_m, is a crucial parameter that determines the temperature range within which a solid can be utilized. A solid with a greater melting temperature has more, higher bonding energy, cohesive energy, and a lower coefficient of thermal expansion. The melting temperature is directly related to the bond strength. Solids can be utilized consistently at temperatures below T_m without experiencing oxidation, chemical alteration, or severe distortion that could lead to mechanical breakdown. The melting temperature calculated using elastic constants can be calculated using the following equation [84].

$$T_m = 354 + 1.5(2C_{11} + C_{33}) \pm 300K \tag{28}$$

The melting temperature of $XGaH_5$ remains consistent due to its identical crystal structure and bonding characteristics. $BaGaH_5$ exhibits the highest melting temperature compared to the other compounds due to its superior elastic strength. The calculated melting temperature for $XGaH_5$ hydrides is quite low, indicating their relatively soft nature.

Thermal conductivity is a crucial attribute that depends on the acoustic wave velocity of a material and describes its capacity to conduct heat. As temperature rises, thermal conductivity falls until it reaches a minimum value at high temperatures. The minimal thermal conductivity, K_{min}, of a solid can be determined using the following equation [85].

$$K_{min} = k_B v_m \left(\frac{M}{n\rho N_A}\right)^{-\frac{2}{3}} \tag{29}$$

The minimal thermal conductivity obtained were 0.68 W m^{-1} K^{-1} for $MgGaH_5$, 0.59 W m^{-1} K^{-1} for $CaGaH_5$, and 0.51 W m^{-1} K^{-1} for $BaGaH_5$. The result for $MgGaH_5$ exceeded that of $CaGaH_5$ and $BaGaH_5$.

3.7. Electronic properties

To obtain a comprehensive study of the electronic properties of $XGaH_5$, its band diagram and Partial Density of State (PDOS) were studied along the axes of high symmetry, as shown in Fig. 5. The Fermi energy level was set to 0 eV and indicated by the red dashed line. Electronic properties provide information about whether materials have metallic, semiconductor, or insulating properties [86,87]. As can be seen from Fig. 5, $BaGaH_5$, $CaGaH_5$, and $MgGaH_5$ have band gap values of 3.08 eV, 4.05 eV, and 3.61 eV, respectively. Due to these high band gaps, all three compounds have an insulating character. Fig. 5 also shows the total and partial densities of states (TDOS and PDOS) for $XGaH_5$ hydrides.

As seen in Fig. 5 a, the largest contribution below the Fermi Energy level between (0 eV) and (−8 eV) comes from the H-1s state. Above the Fermi Energy level, (4 eV)-(5 eV) came from Mg-3s, while (5 eV)-(8 eV) came from Ga-4p. In Fig. 5 b, the largest contribution below the Fermi Energy level between (0 eV) and (−2 eV) comes from the H-1s state. Above the Fermi Energy level, the largest contribution between (4 eV) and (8 eV) came mostly from Ga-4p. Finally, in Fig. 5 c, the largest contribution below the Fermi Energy level between (0 eV) and (−2 eV) comes from the H-1s state. Above the Fermi Energy level, the largest contribution between (3 eV)-(8 eV) came mostly from Ga-4p.

3.8. Hydrogen storage properties

The gravimetric storage capacity ($C_{wt\%}$) and the desorption temperature (T_{des}) of hydrides, or prospective hydrogen storage materials, are two crucial parameters. $C_{wt\%}$ refers to the amount of hydrogen that can be stored per unit weight of the material, while Tdes indicates the temperature at which the hydrogen can be released from the material. These properties are crucial in determining the efficiency and practicality of a hydride as a hydrogen storage solution. A high $C_{wt\%}$ and a low T_{des} are ideal characteristics for a hydride material, as they allow for a greater amount of hydrogen to be stored and released at manageable temperatures. The gravimetric storage capacity is calculated using the following equation [4,34,55,88].

$$C_{wt\%} = \left(\frac{\left(\frac{H}{M}\right)M_H}{M_{Host} + \left(\frac{H}{M}\right)M_H}\, x\, 100\right)\% \tag{30}$$

The molecular weight of hydrogen is represented by the symbol M_H in this equation, the molecular weight of the host material is represented by M_{Host}, and the ratio of hydrogen to metal is indicated by the H/M

Table 8
Calculated crystal density (ρ in g/cm^3), longitudinal, transverse, and average sound velocities (v_t, v_l, and v_m in m/s), Debye temperature, θ_D (K), minimum thermal conductivity, K_{min} (W/mK) for $XGaH_5$ (X = Mg, Ca, Ba) hydrides.

Compound	ρ	v_t	v_l	v_m	T_m	θ_D	K_{min}
$MgGaH_5$	1.80	2485.13	3944.91	2735.24	520.26	345.96	0.68
$CaGaH_5$	1.96	2249.56	3515.08	2471.53	511.44	306.24	0.59
$BaGaH_5$	3.50	1955.63	3395.15	2171.56	542.19	265.83	0.51

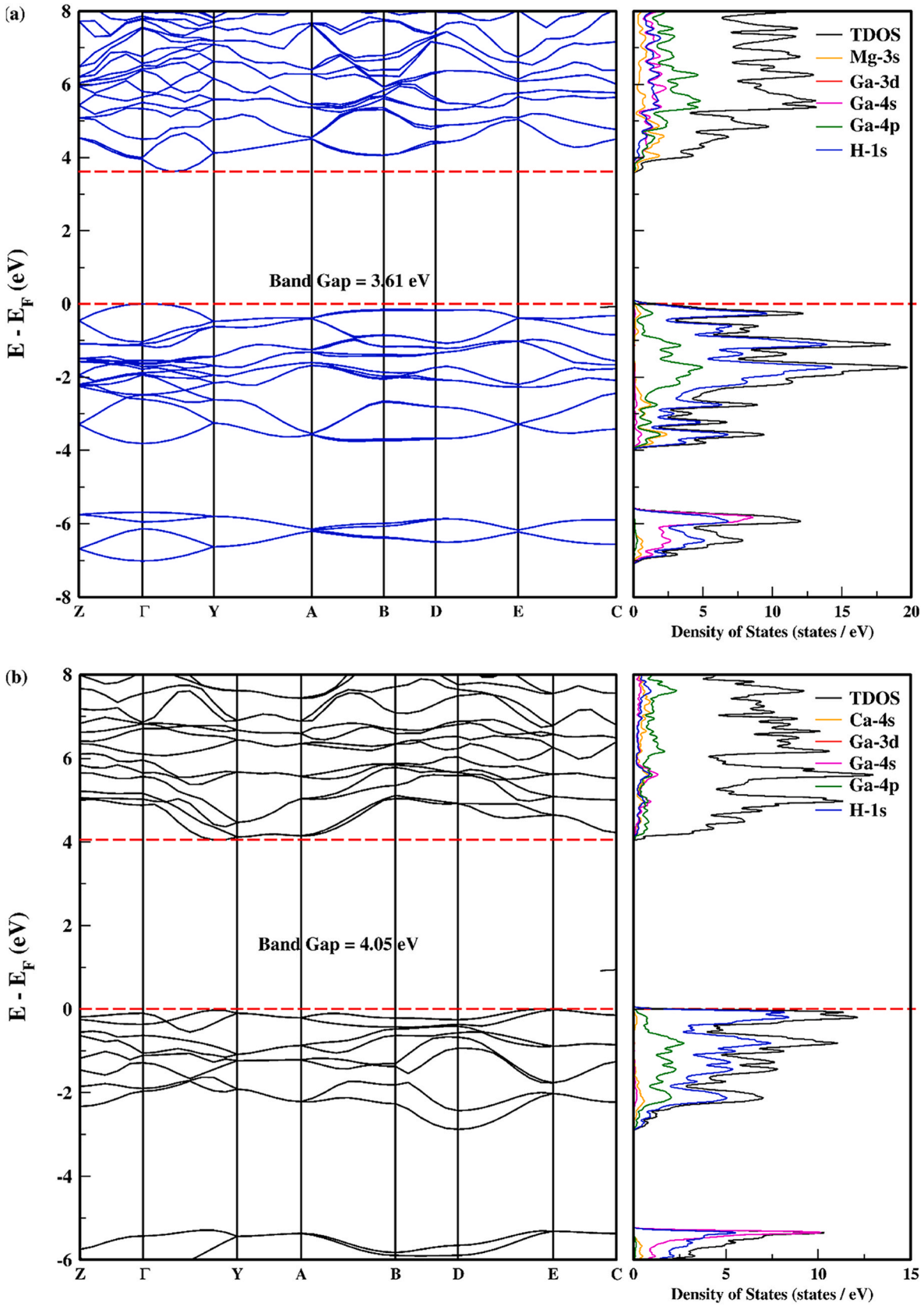

Fig. 5. Electronic bant structure with PDOS for (a) $MgGaH_5$, (b) $CaGaH_5$, and (c) $BaGaH_5$ compounds.

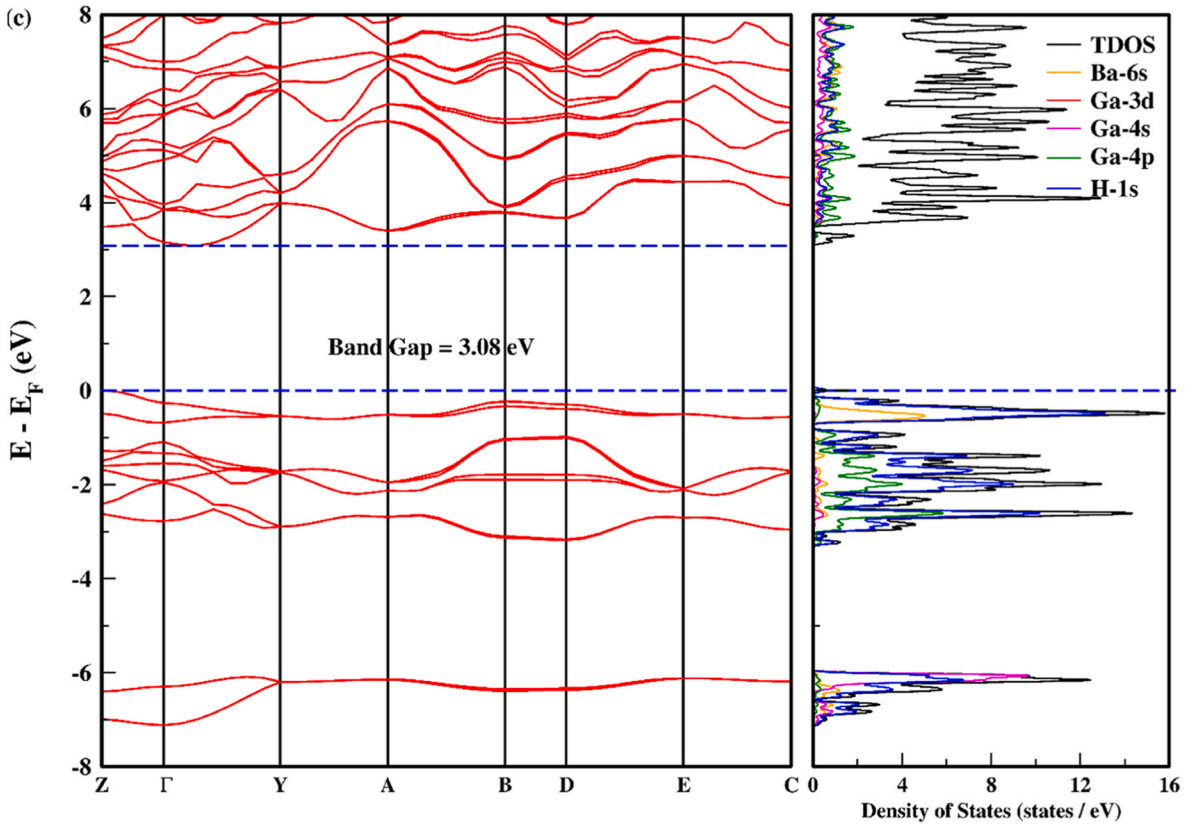

Fig. 5. (*continued*).

symbol. The $MgGaH_5$ 5.1 wt%, $CaGaH_5$ 4.4 wt%, and $BaGaH_5$ 2.38 wt% have estimated gravimetric capacities, respectively. In addition, the volumetric storage capacities of the studied materials were also calculated. Volumetric storage capacities (gH_2l^{-1}) were obtained as 90.95 for MgGaH5, 85.51 for CaGaH5, and 82.46 for BaGaH5. US-DOE's target for 2025 is a gravimetric storage capacity of 5.5 and a volumetric storage capacity of 40. For practical applications, the obtained value of gravimetric storage capacity for $MgGaH_5$ is more close the US Energy Department's aim of 5.5% [32].

Besides gravimetric storage capability, another important parameter for hydrogen storage materials is desorption temperature. The temperature can be estimated using the conventional Gibbs formula, as illustrated in the equations below:

$$\Delta G = \Delta H - T_{des}\Delta S \tag{31}$$

Here ΔH is the enthalpy of the reaction and is calculated as follows $\Delta H = \sum_{products} E - \sum_{reactants} E$. Under normal conditions of pressure and temperature, where $\Delta G = 0$, we can determine T_{des} using the equation [89]:

$$T_{des} = \frac{\Delta S}{\Delta H} \tag{32}$$

The entropy change of hydrogen, denoted as ΔS, is reported as −130.7 J/mol. K in prior research [90]. The desorption temperature values for $MgGaH_5$, $CaGaH_5$, and $BaGaH_5$ are 29.05K, 175.56K, and 218.36K, respectively. The desorption temperature results we obtained are lower than the required T_{des} (233–333 K) range determined by the United States Department of Energy for the year 2025 [6,91].

These materials, which have not been previously reported, can be used as a reference for future theoretical investigations and as a guide for practical synthesis and characterization for hydrogen storage and optoelectronics applications.

4. Conclusions

The goal of this study is to find new and creative compounds that meet the requirements for hydrogen storage. Getting good at storing hydrogen is a tough step for real-world uses. As a result, elements with high kinetics, fast response, and maximum storage capacity are required. Density Functional Theory is used in ab initio study to explain the structural, elastic, thermo-physical, optic, and electronic properties of $XGaH_5$ compounds. The compound's ductile and anisotropic nature is demonstrated by its elastic constants and anisotropic properties, respectively. Band structure investigation of $XGaH_5$ shows insulator properties. PDOS plots, which helped figure out what the energy bands were made of, are being used in more detailed analyses. Moreover, the formation energy of $XGaH_5$ is computed to prove its stability. All compounds are stable because they have a negative enthalpy of formation. The Debye temperatures for $MgGaH_5$, $CaGaH_5$, and $BaGaH_5$ are 345.96 K, 306.24 K, and 265.83 K, respectively. Optical calculations show that $XGaH_5$ exhibits high absorption to far ultraviolet radiation from vacuum, making it a promising optoelectronic material.

No experimental and detailed theoretical data are available on the structural, elastic, thermo-physical, electronic, and optical properties of these compounds. Hence, the results of this study will be beneficial for future experimental investigations and could make a substantial impact on research in the field of hydrogen storage applications.

CRediT authorship contribution statement

Çağatay Yamçıçır: Writing – original draft, Methodology, Investigation. **Cihan Kürkçü:** Writing – original draft, Supervision, Methodology, Investigation.

Declaration of competing interest

The authors declare that they have no known competing financial interests or personal relationships that could have appeared to influence the work reported in this paper.

References

[1] Ali M, Munir J, Khan MJI, Yousaf M, Younis MW, Saeed MA. CO adsorption on two-dimensional 2H-ZrO2 and its effect on the interfacial electronic properties: implications for sensing. Phys Scripta 2023;98:115801. https://doi.org/10.1088/1402-4896/acfa42.

[2] Ali M, Bibi Z, Younis MW, Mubashir M, Iqbal M, Usman Ali M, Asif Iqbal M. An accurate prediction of electronic structure, mechanical stability and optical response of BaCuF3 fluoroperovskite for solar cell application. Sol Energy 2024;267:112199. https://doi.org/10.1016/j.solener.2023.112199.

[3] Ali M, Bibi Z, Mubashir M, Younis MW, Afzal U, El-marghany A. A computational investigation of lithium-based metal hydrides for advanced solid-state hydrogen storage. ChemistrySelect 2024;9:e202304582. https://doi.org/10.1002/slct.202304582.

[4] Al S, Kurkcu C, Yamcicier C. High pressure phase transitions and physical properties of Li2MgH4; implications for hydrogen storage. Int J Hydrogen Energy 2020;45:4720–30.

[5] Ali M, Ain Q, Alkadi M, Munir J, Bibi Z, Younis MW, Ahmed AAA, Mubashir M, Qaid SMH. First-principles evaluation of LiCaF3-αHα as an effective material for solid-state hydrogen storage. J Energy Storage 2024;83:110731. https://doi.org/10.1016/j.est.2024.110731.

[6] Mubashir M, Ali M, Bibi Z, Younis MW, Muzamil M. Efficient hydrogen storage in LiMgF3: a first principle study. Int J Hydrogen Energy 2024;50:774–86.

[7] Ali M, Bibi Z, Younis MW, Majeed K, Afzal U, Khan S, Alotaibi NH, Mubashir M. Enhancement of hydrogen storage characteristics of Na2CaH4 hydrides by introducing the Mg and Be dopant: a first-principles study. Int J Hydrogen Energy 2024;70:579–90. https://doi.org/10.1016/j.ijhydene.2024.05.169.

[8] Mubashir M, Ali M, Bibi Z, Afzal U, Albaqami MD, Mohammad S, Muzamil M. Computational evaluation of novel XCuH3 (X = Li, Na and K) perovskite-type hydrides for hydrogen storage applications using LDA and GGA approach. J Mol Graph Model 2024;131:108808. https://doi.org/10.1016/j.jmgm.2024.108808.

[9] Schlapbach L, Züttel A. Hydrogen-storage materials for mobile applications. Nature 2001;414:353–8. https://doi.org/10.1038/35104634.

[10] A Nickel Metal Hydride Battery for Electric Vehicles | Science, (n.d.). https://www.science.org/doi/abs/10.1126/science.260.5105.176 (accessed March 12, 2024).

[11] Advanced hydrogen storage alloys for Ni/MH rechargeable batteries - Journal of Materials Chemistry (RSC Publishing), (n.d.). https://pubs.rsc.org/en/content/articlelanding/2003/3j/c0jm01921f/unauth (accessed March 12, 2024).

[12] Cao Z, Ouyang L, Li L, Lu Y, Wang H, Liu J, Min D, Chen Y, Xiao F, Sun T, Tang R, Zhu M. Enhanced discharge capacity and cycling properties in high-samarium, praseodymium/neodymium-free, and low-cobalt A2B7 electrode materials for nickel-metal hydride battery. Int J Hydrogen Energy 2015;40:451–5. https://doi.org/10.1016/j.ijhydene.2014.11.016.

[13] NMR study of hydrogen diffusion and phase determination of the Mg2NiHx system | The Journal of Chemical Physics | AIP Publishing, (n.d.). https://pubs.aip.org/aip/jcp/article-abstract/73/10/4758/793721/NMR-study-of-hydrogen-diffusion-and-phase (accessed March 12, 2024).

[14] Blomqvist H, Rönnebro E, Noréus D, Kuji T. Competing stabilisation mechanisms in Mg2NiH4. J Alloys Compd 2002;330–332:268–70. https://doi.org/10.1016/S0925-8388(01)01637-1.

[15] Fujii H, Orimo S, Ikeda K. Cooperative hydriding properties in a nanostructured Mg2Ni–H system. J Alloys Compd 1997;253–254:80–3. https://doi.org/10.1016/S0925-8388(96)03058-7.

[16] Orimo S, Fujii H. Effects of nanometer-scale structure on hydriding properties of Mg-Ni alloys: a review. Intermetallics 1998;6:185–92. https://doi.org/10.1016/S0966-9795(97)00064-2.

[17] Tessier P, Akiba E. Decomposition of nickel-doped magnesium hydride prepared by reactive mechanical alloying. J Alloys Compd 2000;302:215–7. https://doi.org/10.1016/S0925-8388(99)00684-2.

[18] Li C, Zhang X, Wang F. Influence of TM elements on the mechanical and thermodynamic properties of Hf2Si intermetallics. Vacuum 2024;220:112793. https://doi.org/10.1016/j.vacuum.2023.112793.

[19] Wang K, Zhang X, Wang F. Exploring the electronic, mechanical, anisotropic and optical properties of the Sc-Al-C MAX phases from a first principles calculations. Chem Phys Lett 2024;836:141024. https://doi.org/10.1016/j.cplett.2023.141024.

[20] Li C, Zhang X, Wang F. The lattice vibration, mechanical anisotropy, stress-strain behavior and electronic properties of HfxSiy phases: a first-principles study. Vacuum 2023;212:112012. https://doi.org/10.1016/j.vacuum.2023.112012.

[21] Tian M, Zhang X, Wang F. Structural, mechanical, electronic and thermodynamic properties of YBC, YB2C, YB2C2, Y2B3C2 intermetallics. Mater Today Commun 2024;39:108696. https://doi.org/10.1016/j.mtcomm.2024.108696.

[22] Klaveness A, Swang O, Kjekshus A, Fjellvåg H. Coordination preference of Ga in hydrides. Inorg Chem 2006;45:10698–701. https://doi.org/10.1021/ic0616232.

[23] Ordejón P, Artacho E, Soler JM. Self-consistent order-N density-functional calculations for very large systems. Phys Rev B 1996;53:R10441–4. https://doi.org/10.1103/PhysRevB.53.R10441.

[24] Perdew JP, Burke K, Ernzerhof M, Perdew Burke, Reply Ernzerhof. Phys Rev Lett 1998;80. https://doi.org/10.1103/PhysRevLett.80.891. 891–891.

[25] Troullier N, Martins JL. Efficient pseudopotentials for plane-wave calculations. Phys Rev B 1991;43:1993–2006. https://doi.org/10.1103/PhysRevB.43.1993.

[26] Monkhorst HJ, Pack JD. Special points for Brillouin-zone integrations. Phys Rev B 1976;13:5188–92. https://doi.org/10.1103/PhysRevB.13.5188.

[27] Momma K, Izumi F. VESTA: a three-dimensional visualization system for electronic and structural analysis. J Appl Crystallogr 2008;41:653–8. https://doi.org/10.1107/S0021889808012016.

[28] Wallace DC, Callen H. Thermodynamics of crystals. Am J Phys 1972;40:1718–9. https://doi.org/10.1119/1.1987046.

[29] Jain A, Ong SP, Hautier G, Chen W, Richards WD, Dacek S, Cholia S, Gunter D, Skinner D, Ceder G, Persson KA. Commentary: the Materials Project: a materials genome approach to accelerating materials innovation. Apl Mater 2013;1:011002. https://doi.org/10.1063/1.4812323.

[30] Klaveness A, Swang O, Kjekshus A, Fjellvåg H. Coordination preference of Ga in hydrides. Inorg Chem 2006;45:10698–701. https://doi.org/10.1021/ic0616232.

[31] Al S, Cavdar N, Arikan N. Computational evaluation of comprehensive properties of MgX3H8 (X = Sc, Ti and Zr) as effective solid state hydrogen storage materials. J Energy Storage 2024;80:110402. https://doi.org/10.1016/j.est.2023.110402.

[32] Al S, Kurkcu C, Yamcicier C. Structural evolution, mechanical, electronic and vibrational properties of high capacity hydrogen storage TiH4. Int J Hydrogen Energy 2020;45:30783–91.

[33] Gencer A, Surucu G. Investigation of structural, electronic and lattice dynamical properties of *XNiH3* (*X = Li, Na* and *K*) perovskite type hydrides and their hydrogen storage applications. Int J Hydrogen Energy 2019;44:15173–82. https://doi.org/10.1016/j.ijhydene.2019.04.097.

[34] Surucu G, Gencer A, Candan A, Gullu HH, Isik M. CaXH3 (X = Mn, Fe, Co) perovskite-type hydrides for hydrogen storage applications. Int J Energy Res 2020;44:2345–54. https://doi.org/10.1002/er.5062.

[35] Surucu G, Candan A, Gencer A, Isik M. First-principle investigation for the hydrogen storage properties of NaXH3 (X= Mn, Fe, Co) perovskite type hydrides. Int J Hydrogen Energy 2019;44:30218–25. https://doi.org/10.1016/j.ijhydene.2019.09.201.

[36] Dahbi S, Tahiri N, El Bounagui O, Ez-Zahraouy H. Importance of spin-orbit coupling on photovoltaic properties of Pb-free vacancy ordered double perovskites halides X_2TeY_6 (X = Cs , Rb , and Y = I , Br , Cl): first-principles calculations. Intl J of Energy Research 2022;46:8433–42. https://doi.org/10.1002/er.7631.

[37] Soboyejo W. Mechanical properties of engineered materials. CRC press; 2002. https://www.taylorfrancis.com/books/mono/10.1201/9780203910399/mechanical-properties-engineered-materials-wole-soboyejo. [Accessed 2 March 2024].

[38] Pelleg J. Mechanical properties of materials. Dordrecht: Springer Netherlands; 2013. https://doi.org/10.1007/978-94-007-4342-7.

[39] Mouhat F, Coudert F-X. Necessary and sufficient elastic stability conditions in various crystal systems. Phys Rev B 2014;90:224104. https://doi.org/10.1103/PhysRevB.90.224104.

[40] Alam MA, Parvin F, Naqib SH. Ab-initio insights into the pressure dependent physical properties and possible high-Tc superconductivity in monoclinic and orthorhombic MgVH6. http://arxiv.org/abs/2211.09457. [Accessed 2 March 2024].

[41] Rahman F, Ali MM, Ali MA, Uddin MM, Naqib SH, Hossain MM. DFT approach into the physical properties of MTe3 (M= Hf, Zr) superconductors: a comprehensive study. AIP Adv 2023;13. https://pubs.aip.org/aip/adv/article/13/8/085126/2907909. [Accessed 2 March 2024].

[42] Wang P, Zhang N-C, Jiang C-L, Liu F-S, Liu Z-T, Liu Q-J. Structural, mechanical, and electronic properties of Zr–Te compounds from first-principles calculations. Chin Phys B 2020;29:076201.

[43] Kleinman L. Deformation potentials in silicon. I. Uniaxial strain. Phys Rev 1962;128:2614.

[44] Anderson OL, Demarest Jr HH. Elastic constants of the central force model for cubic structures: polycrystalline aggregates and instabilities. J Geophys Res 1971;76:1349–69.

[45] Pettifor DG. Theoretical predictions of structure and related properties of intermetallics. Mater Sci Technol 1992;8:345–9.

[46] Hill R. First-principles elastic constants for the hcp transition metals Fe, Co, and Re at high pressure. Proc Phys Soc 1952:350.

[47] Voigt W. Lehrbuch der kristallphysik (mit ausschluss der kristalloptik). Leipzig; Berlin, Ann Arbor, Mich.: BG Teubner [JW Edwards; 1946.

[48] Reuss A. ZAMM-journal of applied mathematics and mechanics. Zeitschrift Fur Angewandte Mathematik Und Mechanik 1929;9:49.

[49] Ali M, Bibi Z, Younis MW, Majeed K, Iqbal MA. First-principles investigation of structural, mechanical, and optoelectronic properties of Hf2AX (A=Al, Si and X=C, N) MAX phases. J Am Ceram Soc 2024;107:2679–92. https://doi.org/10.1111/jace.19567.

[50] Pugh SF. XCII. Relations between the elastic moduli and the plastic properties of polycrystalline pure metals. London, Edinburgh Dublin Phil Mag J Sci 1954;45:823–43.

[51] Wortman JJ, Evans RA. Young's modulus, shear modulus, and Poisson's ratio in silicon and germanium. J Appl Phys 1965;36:153–6.

[52] Mahamudujjaman M, Afzal MA, Islam RS, Naqib SH. First-principles insights into mechanical, optoelectronic, and thermo-physical properties of transition metal dichalcogenides ZrX2 (X= S, Se, and Te). AIP Adv 2022;12:025011.

[53] Arikan N, Al S, Iyigör A. Mechanical, electronic, thermodynamic and vibrational properties of X2MgAl (X = Sc, Ti and Y) from first principles calculations. J Mol Model 2022;28:366. https://doi.org/10.1007/s00894-022-05358-7.

[54] Iyigör A, Al S, Arikan N. Density functional theory investigation on structural, mechanical, electronic and vibrational properties of Heusler alloys AlXIr2 (X= Co, Cr, Cu, Fe and Zn). Chem Phys Lett 2022;806:140052.

[55] Yamçıçıer Ç. Exploring the structural, elastic, phonon, optoelectronics, and thermoelectric properties of tetragonal complex metal hydride X2MgH4 (X=K, Rb, and Cs) compounds for hydrogen storage applications. Int J Hydrogen Energy 2023. https://doi.org/10.1016/j.ijhydene.2023.09.177.
[56] Naher MI, Afzal MA, Naqib SH. A comprehensive DFT based insights into the physical properties of tetragonal superconducting Mo5PB2. Results Phys 2021;28:104612.
[57] Chen X-Q, Niu H, Li D, Li Y. Modeling hardness of polycrystalline materials and bulk metallic glasses. Intermetallics 2011;19:1275–81.
[58] Vitos L, Korzhavyi PA, Johansson B. Stainless steel optimization from quantum mechanical calculations. Nat Mater 2003;2:25–8.
[59] Phasha MJ, Ngoepe PE, Chauke HR, Pettifor DG, Nguyen-Mann D. Link between structural and mechanical stability of fcc-and bcc-based ordered Mg–Li alloys. Intermetallics 2010;18:2083–9.
[60] Lincoln RC, Koliwad KM, Ghate PB. Morse-potential evaluation of second-and third-order elastic constants of some cubic metals. Phys Rev 1967;157:463.
[61] Islam R, Hossain MM, Ali MA, Uddin MM, Naqib SH. Metallic boro-carbides of A 2 BC (A= Ti, Zr, Hf and W): a comprehensive theoretical study for thermo-mechanical and optoelectronic applications. RSC Adv 2022;12:32994–3007.
[62] Teter DM. Computational alchemy: the search for new superhard materials. MRS Bull 1998;23:22–7.
[63] Tian Y, Xu B, Zhao Z. Microscopic theory of hardness and design of novel superhard crystals. Int J Refract Metals Hard Mater 2012;33:93–106.
[64] Miao N, Sa B, Zhou J, Sun Z. Theoretical investigation on the transition-metal borides with Ta3B4-type structure: a class of hard and refractory materials. Comput Mater Sci 2011;50:1559–66.
[65] Mazhnik E, Oganov AR. A model of hardness and fracture toughness of solids. J Appl Phys 2019;126:125109.
[66] Kube CM. Elastic anisotropy of crystals. AIP Adv 2016;6:095209.
[67] Hossain MM, Hossain MA, Moon SA, Ali MA, Uddin MM, Naqib SH, Islam A, Nagao M, Watauchi S, Tanaka I. NaInX2 (X= S, Se) layered materials for energy harvesting applications: first-principles insights into optoelectronic and thermoelectric properties. J Mater Sci Mater Electron 2021;32:3878–93.
[68] Ranganathan SI, Ostoja-Starzewski M. Universal elastic anisotropy index. Phys Rev Lett 2008;101:055504.
[69] Vahldiek F. Anisotropy in single-crystal refractory compounds. Springer; 2013.
[70] Chung DH, Buessem WR. The elastic anisotropy of crystals. J Appl Phys 1967;38:2010–2.
[71] Ravindran P, Fast L, Korzhavyi PA, Johansson B, Wills J, Eriksson O. Density functional theory for calculation of elastic properties of orthorhombic crystals: application to TiSi 2. J Appl Phys 1998;84:4891–904.
[72] Arsigny V, Fillard P, Pennec X, Ayache N. Fast and simple calculus on tensors in the log-euclidean framework. In: Duncan JS, Gerig G, editors. Medical image computing and computer-assisted intervention – miccai 2005. Berlin, Heidelberg: Springer; 2005. p. 115–22. https://doi.org/10.1007/11566465_15.
[73] Kube CM, De Jong M. Elastic constants of polycrystals with generally anisotropic crystals. J Appl Phys 2016;120:165105.
[74] Wang J, Zhou Y, Liao T, Lin Z. First-principles prediction of low shear-strain resistance of Al 3 BC 3: a metal borocarbide containing short linear BC 2 units. Appl Phys Lett 2006;89:021917.
[75] Ran Z, Zou C, Wei Z, Wang H. VELAS: an open-source toolbox for visualization and analysis of elastic anisotropy. Comput Phys Commun 2023;283:108540. https://doi.org/10.1016/j.cpc.2022.108540.
[76] Dressel M, Grüner G. Electrodynamics of solids: optical properties of electrons in matter. 2002.
[77] Ali M, Yousaf M, Naeem H, Munir J. Layer-sliding-mediated controllable synthetic strategy for the preparation of multifunctional materials. Mater Today Commun 2023;37:107022. https://doi.org/10.1016/j.mtcomm.2023.107022.
[78] Ali M, Yousaf M, Munir J, Khan MJI, ul Ain Q, Younis MW. Controlled dynamic variation of interfacial electronic and optical properties of sodium-intercalated silicene/hBN heterostructure. Eur. Phys. J. Plus 2023;138:1151. https://doi.org/10.1140/epjp/s13360-023-04768-7.
[79] Ali M, Yousaf M, Munir J, Iqbal khan MJ. Achieving controllable multifunctionality through layer sliding. J Mol Graph Model 2024;126:108638. https://doi.org/10.1016/j.jmgm.2023.108638.
[80] Ali M, Bibi Z, Younis MW, Asif Iqbal M. Structural, optoelectronic and thermodynamical insights into 2H-ZrO2: a DFT investigation. Inorg Chem Commun 2024;160:111891. https://doi.org/10.1016/j.inoche.2023.111891.
[81] Hossain A, Sarker MSI, Khan MKR, Rahman MM. Spin effect on electronic, magnetic and optical properties of spinel CoFe2O4: a DFT study. Mater Sci Eng, B 2020;253:114496.
[82] Anderson OL. A simplified method for calculating the Debye temperature from elastic constants. J Phys Chem Solid 1963;24:909–17.
[83] Schreiber E, Anderson OL, Soga N, Bell JF. Elastic constants and their measurement. 1975. https://asmedigitalcollection.asme.org/appliedmechanics/article-abstract/42/3/747/388078. [Accessed 20 December 2023].
[84] Brown LD, Fine ME, Marcus HL. Elastic constants versus melting temperature in metals. Scripta Metall 1984;18:951–6.
[85] Clarke DS. Communicative intent and conventionality. In: Sign levels. Springer; 2003. p. 67–93.
[86] Mubashir M, Ali M, Ain Q, Khan MA, Ghaithan HM, Bibi Z, Aldwayyan AS, Ahmed AAA, Qaid SMH. First-principles screening of XSbF3 (X = Ba and Ra) fluoroperovskites: an insight into structural, optoelectronic and thermal properties. Phys Scripta 2024;99:0659b3. https://doi.org/10.1088/1402-4896/ad46c1.
[87] Mubashir M, Bibi Z, Ali M, Muzamil M, Afzal U, Albaqami MD. First-principles prediction of antimony based XSbF3 (X = Be, Mg, Ca and Sr) fluoroperovskites: an insight into structural, optoelectronic and thermal properties. Phys B Condens Matter 2024;685:415986. https://doi.org/10.1016/j.physb.2024.415986.
[88] Song R, Chen Y, Chen S, Xu N, Zhang W. First-principles to explore the hydrogen storage properties of XPtH3 (X= Li, Na, K, Rb) perovskite type hydrides. Int J Hydrogen Energy 2024;57:949–57.
[89] Al S. Mechanical and electronic properties of perovskite hydrides LiCaH $$ _ {\mathrm {{3}}} $$3 and NaCaH $$ _ {\mathrm {{3}}} $$3 for hydrogen storage applications. Eur Phys J B 2021;94:1–9.
[90] Züttel A. Materials for hydrogen storage. Mater Today 2003;6:24–33.
[91] Lyu J, Elman R, Svyatkin L, Kudiiarov V. Theoretical and experimental research of hydrogen storage properties of Mg and Mg-Al hydrides. J Alloys Compd 2023;938:168618.